Additions to Derck's paper

Asif ud-Doula & David H. Cohen

2 August 2007

1   X-RAY MODELING

We extracted the dispersed HETGS spectra using the processing tools in CIAO v.3.3 (caldb v.3.2), and found that the first order MEG spectrum (-1 and +1 orders) was the only one with a high enough signal to be of use. *Co-authors: We could eliminate the previous sentence since it's covered in §2 of the manuscript. If we do, this next sentence should be incorporated.* We produced a background spectrum from the standard regions, and custom made response matrix files and grating ARFs.

The spectrum qualitatively resembles those of other normal O stars, with wind-broadened lines that look only marginally asymmetric and shifted (see Figure *1 in the present manuscript*). In this section, we subject the strongest lines in the spectrum to quantitative analysis in order to extract information about the hot plasma on ξ Per. The diagnostics we employ include (1) line profile fitting, to derive the spatial distribution of the hot plasma and the optical depth of the overlying, cool wind; and (2) forbidden-to-intercombination line ratio fitting to independently constrain the location of the hot plasma with respect to the photosphere. All of the analysis was performed in XSPEC v.11.3, with custom-written models.

To constrain the location and kinematics of the hot, presumably shock-heated, plasma in the wind, we fit a simple, empirical X-ray emission line profile model, as described in Owocki & Cohen (2001). Aside from the overall normalization, the free parameters of this model are $R_{\rm o}$, the radius below which there is no hot plasma, and $\tau_* \equiv \frac{\dot{M}\kappa}{4\pi R_* v_\infty}$, which is a fiducial wind optical depth. The opacity, κ, is due to bound-free K-shell photoelectric absorption by low-Z metals and helium in the bulk, unshocked portion of the wind. By constraining τ_* from fitting individual line profiles, the mass-loss rate of the wind can be inferred. The model assumes that the emission of X-ray line photons in the numerous shock heated regions in the wind at $r > R_{\rm o}$ can be treated as being smoothly distributed througout the wind, with a constant volume filling factor (which is much less than unity) and with an emissivity that simply scales as the square of the density of the steady-state wind. We note that while this empirical model is inspired by the line-driven instability (Owocki et al. 1988), it makes no assumptions about the mechanisms that heat and cool the X-ray emitting plasma and is flexible enough to encompass many different types of shock models.

The three strongest, unblended lines in the MEG spectrum of ξ Per are the Lyα lines of neon and oxygen, and the neon-like iron line near 15 Å. We fit each of these lines individually with the wind profile model and a weak continuum

Table 1. Wind profile model fit parameters.

Ion	$\lambda_{\rm o}$ (Å)	$R_{\rm o}$ (R_*)	τ_*
O VIII	18.969	$1.62^{+.11}_{-.08}$	$0.27^{+.16}_{-.19}$
Fe XVII	15.014	$1.47^{+.09}_{-.08}$	$0.11^{+.13}_{-.09}$
Ne X	12.134	$1.62^{+.13}_{-.12}$	$0.34^{+.19}_{-.09}$

under it. We fit the continuum level for each line first, in a line free region on either side of the line in question. The results of these three lines fits are summarized in Table 1, and the best-fit models are shown, overplotted on the coadded MEG $\pm$1 data, in Figure 1. All of the fits are statistically good; none have rejection probabilities above 90%. We used the C statistic (Cash 1979) to assess goodness of fit, and also to place uncertainties on the fitted model parameters. The uncertainties listed in Table 1 represent 68% confidence limits. We performed these fits both accounting for and neglecting the very low background spectrum, and found that it had no effect on the derived model parameters.

As can be seen in Figure 1, the lines, though broad, are only marginally skewed. The skewness is caused by the preferential attenuation of redshifted photons from the back of the wind, and thus the very modest degree of skewness seen in the data indicates low levels of attenuation. This is confirmed by the constrains on τ_*, as listed in Table 1. The fits for all three lines are consistent with a value of $\tau_* \approx 0.25$. Using the values of R$_*$, v_∞, and $\dot{M}$ from Repolust et al. (2004), and an X-ray opacity of $\kappa = 70$ cm^2 g^{-1} at 15 Å, which is consistent with model calculations found in the literature (Cohen et al. 1996; Waldron et al. 1998)[1], we would expect $\tau_* = 1.6$. Finding values that are 5 to 10 times below this is consistent with what is found from detailed analysis of the line profiles of other O stars, such as ζ Pup (Kramer et al. 2003) and ζ Ori (Cohen et al. 2006). The profiles observed in ξ Per are indeed even less asymmetric than those measured in these two O supergiants, but the mass-loss rate of ξ Per is correspondingly lower, so that is to be expected. In fact, the theoretically expected value of τ_*

---

[1] A modest wavelength dependence in the X-ray opacity is expected over the range of the three lines under consideration here. But detailed modeling, which is beyond the scope of this paper, is required to determine exactly what this variation looks like. Specifically, the location and strengths of K-shell edges of N and O and L-shell edges of Fe, which depend on wind abundances and ionization balance, will tend to flatten out the canonical wavelength-dependence of bound-free opacity.
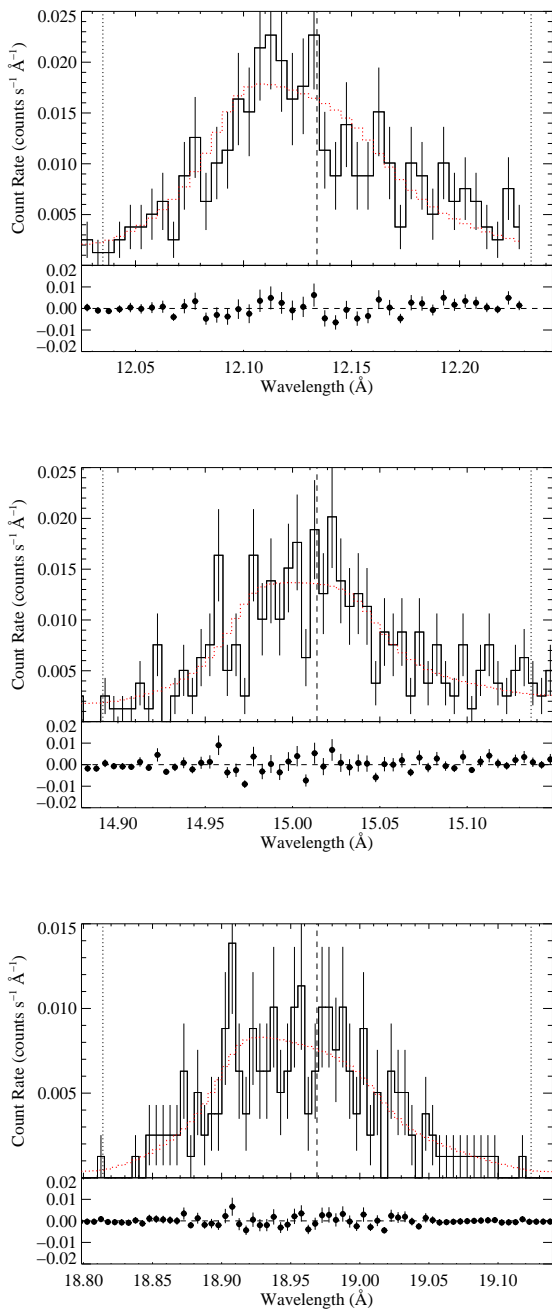
Figure 1. The best-fit wind profile models, to three of the strongest lines in the MEG ±1 spectrum (negative and positive orders coadded in this figure): Ne x Lyα at 12.134 Å, Fe xvii at 15.014 Å, and O viii Lyα at 18.969 Å. The vertical dashed line indicates the laboratory rest wavelength for each emission line, while the dotted lines represent the Doppler shift associated with the wind terminal velocity.

is 6.4 times smaller for ξ Per than for ζ Pup, when we take the parameters for ζ Pup from the same sources (including the Hα mass-loss rate of $8.7 \times 10^{-6}\ M_{\odot}\ yr^{-1}$ from Repolust et al. (2004)). And the values of τ_* from the fits to the ξ Per data we present here are indeed about six times smaller than those found for ζ Pup (Kramer et al. 2003; Cohen et al.

2007). So the line profiles in the X-ray spectrum of ξ Per correspond quantitatively to those observed in ζ Pup.

The simplest interpretation of the small derived values of τ_* is that the mass-loss rate of ξ Per is actually approximately six times lower than that inferred from the strength of the star's Hα emission under the assumption of a smooth wind. This is consistent with the observations and theoretical expectations for clumping in hot star winds, which, if unaccounted for, will lead to an overestimate of wind mass-loss rates (Bouret et al. 2003; Fullerton et al. 2006; Puls et al. 2006). Note that the factor of roughly six reduction in the mass-loss rate is in line with what X-ray observations of other O stars are telling us. Extreme porosity could also conceivably account for the relative symmetry and lack of skewness of the observed line profiles in the *Chandra* spectrum of ξ Per (Oskinova et al. 2006; Owocki & Cohen 2006), but this would require a porosity length (roughly equivalent to the interclump spacing) in excess of a stellar radius.

The values we derive for $R_{\rm o}$ from the line fits are also consistent with what is observed in other O stars (Kramer et al. 2003; Cohen et al. 2006). Having X-ray emission only above about half a stellar radius in the winds of O stars is what is seen in numerical simulations and is expected theoretically, because of the suppression of the wind instability due to the strong scattered photospheric radiation in the dense base of the wind (Feldmeier et al. 1997).

We can place additional independent constraints on the spatial distribution of the shock-heated plasma in the wind of ξ Per by analyzing the ratio of the forbidden-to-intercombination line strengths in the helium-like species observed in the MEG spectrum. This line ratio is sensitive to the distance of the hot plasma from the photosphere because electrons in the upper level of the forbidden line can be photoexcited to the upper level of the intercombination line (really two closely spaced levels) if the photospheric UV mean intensity at the location of the X-ray emitting plasma is high enough. The energy required for this photoexcitation is roughly 10 eV, and scales with the atomic number of the element. Thus, if one knows the emergent photospheric flux in the UV, the line ratio provides information about the distance via its sensitivity to the UV mean intensity in the wind. The closer the X-ray emitting plasma is to the photosphere, the higher the photoexcitation rate and the weaker the forbidden line in the observed X-ray spectrum.

This diagnostic is often employed in O stars to find a single formation radius of the parent ion of a given line complex (see *e.g.* Kahn et al. (2001)). However, the X-ray emitting plasma is likely distributed throughout the wind, so assuming a single formation radius is an oversimplification. Here we model the f/i ratios in the X-ray spectrum of ξ Per, taking account of the spatial distribution of plasma, as first done by Leutenegger et al. (2006). To do this, we self-consistently fit the same type of wind emission line profile used to fit individual lines, to all three lines in these He-like complexes: the resonance line, the intercombination line, and the forbidden line. The model fits all the lines simultaneously and adjusts the contribution to the forbidden and intercombination lines at each radius to account for the UV photoexcitation that alters the ratio. Thus, this modeling adjusts the line ratio and the individual line profiles in cocert.
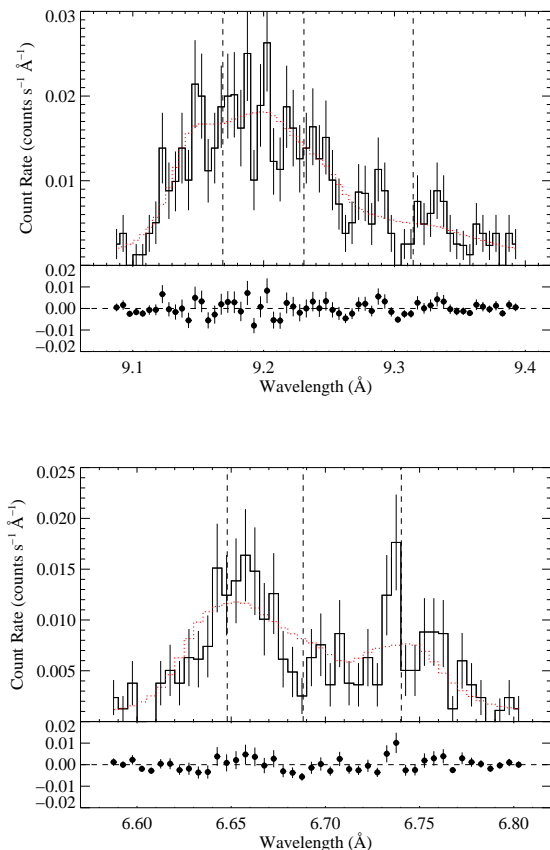
We present fits to the Mg xi and Si xiii complexes, near

Figure 2. The helium-like complexes of Mg (top) and Si (bottom), with the best-fit wind profile models (to all three components of the complex) overplotted. The rest wavelengths of the resonance, intercombination, and forbidden (from blue to red; left to right) lines are indicated in each panel. In collisional equilibrium, with no photoexcitation, the forbidden line is stronger than the intercombination line (by about a factor of three). Here, especially for Mg XI, the intercombination line is stronger than the forbidden line.

9.2 Å and 6.7 Å, respectively. Lower-Z complexes do not provide useful constraints (and the Ne IX complex is blended with iron emission lines in any case), while the higher Z complexes (S XV and above) are too weak in the data to derive any meaningful constraints. We used the same fitting technique as described above for the individual lines - fitting the nearby continuum first, and then fitting the line by minimizing the C statistic to find the best fit model and then assessing the confidence limits on each fitted model parameter using the same statistic. The free parameters of the model are the same as for the model fit to the individual lines, but we stress that now the $R_{\rm o}$ parameter controls not only the line profile shapes but also the ratio of the strength of the forbidden and intercombination lines. The only other parameter of the model is the G ratio, which is the strength of the sum of the forbidden and intercombination line fluxes to that of the resonance line.

In Figure 2 we show the best fit models to the two helium-like complexes. Both fits are good, with the line profiles and the line ratios simultaneously fit for each com-

plex. The best-fit $R_{\rm o}$ values are $1.47^{+.17}_{-.09}$ R$_*$ for Si XIII and $1.64 \pm .10$ R$_*$ for Mg XI. We stress that this parameter is the onset radius of X-ray emission, with contributions to the emission from the entire wind beyond this point weighted as the square of the wind density.

Note that the forbidden line in each complex is broader than the other two lines. This is because forbidden line emission is suppressed by the UV photoexcitation near the star, where the velocity and associated Doppler broadening is small. But far from the star, where the veclocity is high and the contribution to the line profile is strongly Doppler broadened, the forbidden line emissivity is much stronger, and the intercombination line emissivity is correspondingly weaker.

REFERENCES

Bouret, J.-C., Lanz, T., Hillier, D.J., Heap, S.R., Hubeny, I., Lennon, D.J., Smith, L.J., & Evans, C.J. 2003, ApJ, 595, 1182

Cash, W. 1979, ApJ, 228, 939

Cohen, D.H., Cooper, R.G., MacFarlane, J.J, Owocki, S.P., Cassinelli, J.P., & Wang, P. 1996, ApJ, 460, 506

Cohen, D.H., Leutenegger, M.A., Grizzard, K.T., Reed, C.L., Kramer, R.H., & Owocki, S.P. 2006, MNRAS, 368, 1905

Cohen, D.H., Leutenegger, M.A., ud-Doula, A., Townsend, R., & Owocki, S.P. 2007, Procedings of *Clumping in Hot-Star Winds*, Potsdam: Universitäts-Verlag, eds. Hamann, Feldmeier, & Oskinova, in press

Feldmeier, A., Puls, J., & Pauldrach, A.W.A. 1997, A&A, 322, 878

Fullerton, A.W., Massa, D.L., & Prinja, R.K. 2006, ApJ, 637, 1025

Kahn, S., Leutenegger, M.A., Cottam, J., Rauw, G., Vreeux, J.-M., den Boggende, A.J.F., Mewe, R., Güdel, M. 2001, A&A, 365, L312

Kramer, R.H., Cohen, D.H., & Owocki, S.P. 2003, ApJ, 592, 532

Leutenegger, M.A., Paerels, F.B.S., Kahn, S.M., Cohen, D.H. 2006, ApJ, 650, 1096

Oskinova, L.M., Feldmeier, A., & Hamann, W.-R. 2006, MNRAS, 372, 313

Owocki, S.P., Castor, J.I., & Rybicki, G.B. 1988, ApJ, 335, 914

Owocki, S.P. & Cohen, D.H. 2001, ApJ, 559, 1108

Owocki, S.P. & Cohen, D.H. 2006, ApJ, 648, 565

Puls, J., Markova, N., Scuderi, S., Stanghellini, C., Taranova, O.G., Burnley, A.W., & Howarth, I.D. 2006, A&A, 454, 625

Repolust, T., Puls, J., & Herrero, A. 2004, A&A, 415, 349

Waldron, W.L., Corcoran, M.F., Drake, S.A., & Smale, A.P., 1998, ApJ, 118, 217